Volcanic Forcing of Climate over the Past 1500 Years: An Improved Ice-Core-Based Index for Climate Models

Chaochao Gao[1], Alan Robock[1], and Caspar Ammann[2]

[1] Department of Environmental Sciences, Rutgers University, New Jersey, USA
[2] National Center for Atmospheric Research, Boulder, Colorado, USA

Journal of Geophysical Research-Atmospheres

In press

April, 2008

Revised July, 2008

Corresponding Author:
Alan Robock
Department of Environmental Sciences
Rutgers University
14 College Farm Road
New Brunswick, NJ 08901
Phone: 732-932-3891
Fax: 732-932-8644
E-mail: robock@envsci.rutgers.edu

Abstract

Understanding natural causes of climate change is vital to evaluate the relative impacts of human pollution and land surface modification on climate. We have investigated one of the most important natural causes of climate change, volcanic eruptions, by using 54 ice core records from both the Arctic and Antarctica. Our recently collected suite of ice core data, more than double the number of cores ever used before, reduces errors inherent in reconstructions based on a single or small number of cores, which enables us to obtain much higher accuracy in both detection of events and quantification of the radiative effects. We extracted volcanic deposition signals from each ice core record by applying a high-pass LOESS filter to the time series and examining peaks that exceed twice the 31-year running median absolute deviation. We then studied the spatial pattern of volcanic sulfate deposition on Greenland and Antarctica, and combined this knowledge with a new understanding of stratospheric transport of volcanic aerosols to produce a forcing data set as a function of month, latitude, and altitude for the past 1500 years. We estimated the uncertainties associated with the choice of volcanic signal extraction criteria, ice-core sulfate deposition to stratospheric loading calibration factor, and the season for the eruptions without a recorded month. We forced an energy balance climate model with this new volcanic forcing data set, together with solar and anthropogenic forcing, to simulate the large scale temperature response. The results agree well with instrumental observations for the past 150 years and with proxy records for the entire period. Through better characterization of the natural causes of climate change, this new data set will lead to improved prediction of anthropogenic impacts on climate. The new data set of stratospheric sulfate injections from volcanic eruptions for the past 1500 years, as a function of latitude, altitude, and month, is available for download in a format suitable for forcing general circulation models of the climate system.

1. Introduction

The climatic impact induced by volcanic "dust veils" has long been recognized [*Lamb*, 1970; *Toon and Pollack*, 1980]. In particular, volcanic sulfates that form in the stratosphere have been identified as the main cause of large-scale climate perturbations, while the effects of volcanic ash are normally short-lived due to rapid removal. Volcanic aerosol forcing has also been found to be an important cause of observed climate variability in climate model simulations [e.g., *Robock*, 1981; *Gilliland and Schneider,* 1984; *Crowley*, 2000; *Ammann et al.*, 2003; *Wigley et al.*, 2005]. Despite its climatic importance, currently available volcanic forcing indices all have drawbacks, as summarized by *Robock and Free* [1995]. Both Lamb's Dust Veil Index (DVI) [*Lamb*, 1970] and Mitchell's index [*Mitchell*, 1970] were based on rather subjective, and at times even climatic, information; the Volcanic Explosivity Index (VEI) [*Newhall and Self*, 1982] measured the intensity or explosive magnitude of eruptions, a quantity not directly related to the climatic impact potential; the original Sato index [*Sato et al.*, 1993] uses estimates of ejecta volume from *Mitchell* [1970] during for the period 1850-1882, optical extinction data after 1882 (initially from a single, noisy station [*Stothers*, 1996]), and satellite data for the period after 1979. The recent part of this index may be an improvement over the DVI or VEI as it includes actual observations of the latitudinal and temporal extent of the aerosol clouds, however it lacks consistency of its source data - a deficiency particularly problematic when looking at volcanic influence over long time scales - and only goes back to 1850. *Stothers* [1996, 2001] improved on this inconsistency and reconstructed a volcanic optical depth index based on pyrheliometric observations for the period 1881-1960 and stellar extinction observation for 1961-1978. A limitation of most of these indices arises from the fact that events were often only registered when there was a direct eyewitness report of the eruption from the ground. Thus, the problem of missing volcanic eruptions is unavoidable and becomes increasingly severe as we go further

back in time, especially in the Southern Hemisphere (SH). More objective and continuous time series of volcanic eruptions can be obtained from ice core records, since they are direct measures of volcanic sulfate [*Hammer*, 1977; *Hammer*, 1980].

During the past decade, several studies [*Robock and Free,* 1995; *Zielinski* 1995; *Crowley* 2000; *Robertson et al.,* 2001; and *Ammann et al.*, 2003, 2007] have attempted to reconstruct volcanic indices from single or a few ice cores. Among these indices the record by *Crowley* [2000, an update of *Crowley and Kim*, 1999] is the most widely used. This index is based essentially on two well-dated ice core records from Greenland, Crête [*Hammer*, 1980] and GISP2 [*Zielinski et al*., 1995] with some additional information embedded using the Arctic-Antarctic comparisons of *Langway et al.* [1995]. *Ammann et al*. [2007] applied a compilation based on up to 14 high latitude ice core records, among which five came from Antarctica. To combine the individual series into hemispheric composites, both the *Crowley* [2000] and *Amman et al.* [2007] reconstructions applied a suite of somewhat subjective, albeit in principle justifiable, corrections. One necessary correction involved adjustments in the time scales of the series to optimize the joint chronology across cores, and to combine the different types of data (i.e., electric conductivity measures, dielectric properties of ice, and direct sulfate flux measurements) they applied an empirical scaling of the series to selected reference events (Krakatau and Tambora, respectively). *Crowley* [2000] additionally applied a dampening factor for very large events (reducing loadings by the power of 2/3 for events larger than 15 Mt of sulfate) based on the apparent lack of proportional climate impacts in some reconstructions. Such a correction can be justified by the idea that aerosol growth in very large sulfate clouds might be more efficient [*Pinto et al.*, 1989]. Both reconstructions also used the assumption that if anomalous sulfate was found in both hemispheres within a couple of years that a common tropical source was likely [also see *Langway et al.*, 1995]. *Crowley and Kim* [1999] had tested

the climatic impact of this assumption for unknown events by comparing a tropical source with two independent high-latitude events. They found that the effect of such a mis-identification was relatively small. Comparing all available ice-core based series shows general agreement in the depiction of periods of more intense volcanism. The individual peak forcing estimates however differ due to different, and often limited, data sources, particularly with regard to the important direct sulfate measurements [*Robock and Free*, 1996]. Due to the large spatial variability of volcanic deposition on ice sheets, there is the danger that reconstructions based on single or a few ice cores may omit certain events [*Zielinski et al.,* 1995], or they may bias the estimates of the magnitudes for individual eruptions [*Mosley-Thompson et al.*, 2003; *Traufetter et al.*, 2004; *Gao et al.*, 2007]. This points to the importance of using the largest possible ice core dataset to produce a more reliable volcanic index.

During the past 10 years a large number of new ice cores have been recovered, and most of these were analyzed using continuous sulfate measurements [*Cole-Dai et al.* 1997, 2000; *Sommer et al.* 2000; *Bigler et al.* 2002; *Palmer et al.* 2002; *Stenni et al.* 2002; *Budner and Cole-Dai,* 2003; *Dixon et al.* 2004; *Traufetter et al.*, 2004; *Castellano et al.*, 2005; *Kurbatov et al.*, 2006]. This offers the potential for a dramatic improvement in the reconstruction of a volcanic forcing index over the past centuries and millennia. We have worked with the international ice core community and collected, with their generous contributions, a total of 53 ice core series with the goal of developing a comprehensive volcanic forcing time series targeted at applications for state-of-the-art climate model simulations. To generate such a series, a few steps have to be performed:

1. *Volcanic signal extraction*. We extracted the volcanic signals by applying a high pass LOESS filter [*Cleveland*, 1979; *Cleveland and Devlin*, 1988] to remove the background

variation, and examining the potential peaks that exceed a magnitude of twice the local 31-year running median (2x median absolute deviation, 2xMAD) [*Gao et al.*, 2006].

2. *Dating corrections*. As clearly demonstrated in *Gao et al.* [2006], prominent ice core signals of less well documented events, such as the 15th century Kuwae eruption, could be up to 10 years apart. By cross-core comparison, combined with historical records, we can narrow down or sometimes pinpoint the year of eruptions and adjust the chronology of each time series accordingly. Careful time correction provides not only a cleaner eruption chronology but also a more precise alignment required for the quantification of the corresponding magnitudes.

3. *Calculation of Arctic or Antarctic mean volcanic sulfate deposition, taking into account the spatial variation*. *Mosley-Thompson et al.* [2003] found a systematic relationship between the volcanic sulfate deposition and accumulation rate in their six PARCA (Program for Arctic Regional Climate Assessment) ice cores. *Gao et al.* [2007] also found, from 44 ice core sulfate records, that the deposition has a consistent spatial pattern that resembles the general pattern of precipitation distribution. Taking into account such systematic spatial differences, *Gao et al.* [2007] offered a way to adjust the changing ice core networks for individual events and to calculate an Arctic and an Antarctic mean sulfate deposition for large explosive eruptions during the past millennia.

4. *Conversion from ice-core deposition to stratospheric sulfate loading*. *Gao et al.*, [2007] calculated a set of calibration factors from three independent methods: the radioactive deposition from nuclear bomb tests, satellite observations of Pinatubo aerosol loading, and climate model simulations of volcanic sulfate transport and deposition following the 1783 Laki, 1815 Tambora, 1912 Katmai, and 1991 Pinatubo eruptions. The stratospheric aerosol loading we obtained agreed well across the different methods. Thus, here we retained the conversion factors for high and low-latitude events from *Gao et al.* [2007].

Applying this complete protocol, we obtained a history of stratospheric volcanic sulfate mass loading for the past 1500 years. This series can be converted into an optical perturbation index and further into a radiative forcing series that can be used in simple energy balance models. For general circulation models (GCMs), however, a more detailed dataset with latitudinal and vertical information of the evolution of the volcanic aerosol clouds is necessary. As recent studies [*Robock and Mao*, 1992; *Robock*, 2000; *Ammann et al.*, 2003; *Graf et al.*, 2007] have shown, the seasonal evolution of volcanic aerosols might also be important, particularly because of its impact on winter hemisphere temperature gradients which in turn affect atmospheric circulation [*Stenchikov et al.*, 2002]. *Sato et al.* [1993, and updated to present] contains a good compilation of stratospheric volcanic optical depth for the satellite period, but no detailed spatial observations exist prior to the 1970s. *Stothers* [1996, 2001] extended the latitudinal-temporal dependent optical depth index back to the 1880s.

Because aerosol transport is largely driven by the seasonally changing wind patterns in the stratosphere, a simple transport scheme can be applied. *Grieser and Schönwiese* [1999] and *Ammann et al*. [2003, 2007] applied a simple seasonal evolution of aerosol clouds that allows simulation of the spread after any eruption. Ignoring potential modifications due to the phase of the Quasi-Biennial Oscillation (QBO), the resulting mean distribution from such a transport model nevertheless looks realistic and offers the final step in the development of a volcanic dataset appropriate for forcing a GCM.

After briefly introducing the ice core time series in section 2, we summarize in section 3 the development of the hemispheric sulfate loading series, and the simulation of temperature response to the volcanic perturbations for the past millennium using an energy balance model in section 4. Section 5 then transforms these mass emissions history into an evolving volcanic mass and forcing dataset. Despite the significantly enlarged dataset (based on more than double

the number of records previously used), there are still remaining uncertainties, discussed in section 6. We then conclude with the Internet link to the new volcanic forcing dataset.

2. Ice Core Time Series

Figure 1 shows the ice core time series we have collected over the years, from which one can see that our ice core data cover major parts of both Greenland and Antarctica ice sheets. We chose 36 from these ice core time series to be used in this study, excluding time series that were too short or that had large gaps. Table 1 lists the general information and references of these 36 ice core time series. The ice core time series are essentially the same as those used in *Gao et al.*, [2007] except that we also included 10 electrical conductivity measurement (ECM) records to build an event chronology as well as to quantify the corresponding magnitude for each eruption with the various ice core time series. To achieve this goal we adapted a two-step procedure, that is, we first used all of the 36 ice core records in concert to pinpoint the timing of each eruption, and then only the actual sulfate records to calculate the magnitude of ice core volcanic sulfate deposition. The reason we choose not to use ECM records in calculating the volcanic deposition is that ECM measures the acidity caused not only by sulfuric acid (H_2SO_4), but also by nitric (HNO_3), hydrochloric (HCl), and hydrofluoric (HF) acids. Besides, the acidity can be reduced by deposition of basic (as contrasted with acidic) aerosol particles; and the values depend on the temperature at the time when the measurement was taken. Nevertheless, strong ECM peaks do indicate the timing of the arrival of volcanic sulfate to the ice.

Just like *Gao et al.* [2007], we converted all of the actual sulfate records into a flux unit (kg H_2SO_4 km^{-2} a^{-1}). We also combined the sulfate deposition for Laki and Tambora from six PARCA (Program for Arctic Regional Climate Assessment) ice cores [*Mosley-Thompson et al.*, 2003] and 12 Greenland ice cores [*Clausen and Hammer*, 1988] with our ice core results to

obtain a more precise estimate of Greenland ice core sulfate deposition. This gave a total of 54 sulfate ice core records, 36 from this study plus six PARCA and 12 from *Clausen and Hammer*, [1988] , to be used in this study.

3. Calculation of Stratospheric Volcanic Sulfate Injection

The same procedure for calculating the stratospheric sulfate aerosol injection in *Gao et al.*, [2007] (also described in the introduction) was applied to the 36 ice cores to calculate the loading time series for the past 1500 years, with only one exception. That is, instead of calculating the local mean deposition of cores that lie close to each other for each eruption, we calculated a set of ratios between the individual core vs. Greenland or Antarctic mean deposition and applied these ratios globally to individual ice cores before they were used to calculate the Arctic or Antarctic mean depositions. In particular, we selected five large low-latitude eruptions (1809 Unknown, 1815 Tambora, 1883 Krakatau, 1963 Agung, and 1991 Pinatubo) during the past two centuries and calculated the ratios between the volcanic deposition in individual ice cores and that of the Greenland or Antarctic mean for each event. We then calculated the mean ratio for each ice core time series by simply averaging the five ratios. These mean ratios were then applied to each time series before attempting to calculate the Greenland or Antarctic mean deposition to ensure that, on average, the relative contributions from each core would remain the same. By doing so, we reduce the bias caused by having only a few ice core records available in the early period.

Figure 2 shows the resulting time series of stratospheric volcanic sulfate injection for the Northern Hemisphere (NH), SH, and global average for the past 1500 years. We see that the largest stratospheric sulfate aerosol injection events are the 1259 Unknown, 1453 Kuwae, 1815 Tambora eruptions in tropical regions, and the 1783 Laki eruption at high latitude of the NH. The Kuwae sulfate injection was one year later in NH than SH since the peak deposition showed

up a year later in Arctic ice cores. We also found a series of moderate to large sulfate injections during the 13th century, in 1228, 1259, 1268, 1275 and 1285 C.E. The cumulative volcanic sulfate flux in the 13th century was two to 10 times larger than that in any other century within the last millennium.

4. Climate Model Simulation of Temperature Response to Volcanic Eruptions

We simulated the effect of volcanic eruptions on climate for the past 1150 years using our new volcanic forcing together with solar and anthropogenic forcing with the upwelling diffusion energy balance model MAGICC (Model for the Assessment of Greenhouse-gas-Induced Climate Change, *Wigley and Raper* [1992, 2001]). MAGICC was used extensively in the third Intergovernmental Panel on Climate Change assessment and has been tested for its ability to produce the volcanic caused climate response against the National Center for Atmospheric Research/U.S. Department of Energy Parallel Climate Model [*Wigley et al.*, 2005]. The very close agreement found by *Wigley et al.* justifies the use of MAGICC to obtain reliable estimates of how the climate responds to various volcanic eruptions with some confidence.

The input forcing for MAGICC is the global mean monthly radiative forcing at the top of the atmosphere. Therefore, we converted the stratospheric volcanic aerosol loading (in units of Tg) obtained above into radiative forcing by first dividing the loading by 1.5×10^{14} Tg [*Stothers*, 1984] to obtain the optical depth; then multiplying the optical depth by 20 [*Wigley et al.*, 2005] to obtain the radiative forcing in W m^{-2}. The solar forcing over the past 1000 years was obtained by scaling solar modulation estimates [*Muscheler et al.*, 2007] to a recent solar irradiance reconstruction [*Wang et al.*, 2005]. For anthropogenic forcing we applied the IPCC SRES A1B forcing scenario with median anthropogenic aerosol forcing [Q(2000) = 1.4 W m^{-2},

Tom Wigley, personal communication]. The model was run from 850 C.E. to 2015 C.E. with climate sensitivity set to be 3.0°C for doubled CO_2 concentration.

Figure 3 shows the comparison between the model simulated global mean temperature and instrumental observations for the past 150 years. We found a good agreement between the model results and observations. The model accurately simulated the cooling of about 0.2-0.3°C for the three tropical eruptions, 1883 Krakatau, 1963 Agung, and 1991 Pinatubo, during this period. On the other hand, the modeled temperature did not show the sharp warmings in 1878 and the early 1940s. This is because there were large El Niño events then [*Brönnimann et al.*, 2004], which are not included in the energy balance model, and because the temperature drop in August, 1945 is the result of errors in the sea surface temperature record, which still need to be corrected in the record we used and all other records [*Thompson et al.*, 2008].

The model also did not produce cooling for the 1982 El Chichón eruption. This is because the El Chichón signal was missed from our ice-core-based reconstruction because most of our Arctic ice cores end before or around the 1980s, and due to the asymmetric distribution of the El Chichón cloud [*Robock*, 2000], no El Chichón signal was extracted from the Antarctic ice core records. Therefore, in a subsequent MAGICC run we replaced our ice-core-based reconstruction with Sato's [*Sato et al.*, 1993 and updated to present] values after 1970 and compared the model response to NH temperature reconstructions (Fig. 6.10 in *IPCC* [2007]) for the past millennium (Fig. 4). The model simulation generally captured the temperature variation on the decade to century time scale: the (sometimes interrupted) mean temperatures between the 9th and 12th centuries, which were generally warmer than before or after, and only in the 19th century reach similarly warm conditions again; the coldest episodes occurring during the 13th, 15th, and 19th centuries; and the exceptionally high temperature after 1850. Several sharp cooling events mark the temperature response to large explosive volcanic perturbations, for

example, the 1453 Kuwae, 1809 Unknown and 1815 Tambora eruptions. The largest volcanic perturbation was estimated to be that from the 1259 Unknown. Together with four other moderate to large sulfate injections during the century, 1228, 1268, 1275 and 1285, this particularly large eruption caused a clear temperature decrease of several tenths of a degree Celsius for the entire 13th century. This suggests the role of these temporal-closely spaced eruptions may have in century-scale climate variation of that period.

The model produced more cooling than the reconstructions for the 1259 Unknown eruption. There could be multiple reasons for this. On the one hand, IVI2 may overestimate the forcing for large volcanic eruptions due to the linear assumption we made between the atmospheric sulfate mass loading and its radiative perturbation [e.g., *Pinto et al.*, 1989]. The model may be too sensitive to volcanic forcing due to its simplicity. On the other hand, temperature reconstructions also contain significant uncertainties, especially for early periods like the 13th century when the data density (spatial sampling) is severely limited. Besides, *Robock* [2005] showed that temperature reconstructions based on tree ring records tend to underestimate the cooling following volcanic eruptions because of compensating growth from the diffuse radiation caused by volcanic aerosols. The model temperature also appears to be lie at the high end of the proxy reconstruction range during the17th and most of the 19th century, probably because of the low long-term variations in the solar forcing time series we used.

5. Construction of a Monthly and Spatially Dependent Forcing Index

To produce the monthly and spatially dependent volcanic forcing index we applied the *Grieser and Schönwiese* [1999] stratospheric transport parameterization to calculate the horizontal spread of aerosol within the low stratosphere plus a latitude-time dependent function to describe the production and sedimentation of aerosols. We also interpolated the vertical distribution of volcanic aerosols based on information obtained from 11 lidar measurements of

the backscattering coefficient after the 1991 Pinatubo eruption [*Antuña et al.*, 2002], assuming that the aerosols from every eruption have the same vertical distribution as Pinatubo.

We divided each hemisphere into eight equal-area latitude belts (three in the tropics, four in the midlatitudes, and one in high latitude) and applied a non-local diffusion formalism to describe the horizontal transport of aerosols [*Grieser and Schönwiese,* 1999]. The transport coefficients among different latitude belts for different seasons are given in Table 2. Compared to *Grieser and Schönwiese* [1999] we increased the diffusion rate from the tropics to the extratropics and from the extratropics to the polar region, as well as the exchange coefficient within the extratropics during summer and fall to allow more transport of aerosols from low latitudes to high latitudes. The exchange coefficients in *Grieser and Schönwiese* [1999] were obtained from recent studies of stratospheric mass transport and most of the estimates contain uncertainties. We modified a few of the exchange rates within these uncertainty estimates to increase the spread of aerosols from tropics to high latitudes. Another major difference is that for tropical eruptions we put initial sulfate aerosol in each hemisphere (according to ice core estimates) and only allow the transport within each hemisphere, i.e., there is no transport across the Equator between the two lowest latitude belts in the tropics. We adopted this approach because for the early eruptions we have no information about the location or season of the eruption and thus about the hemispheric partitioning of the sulfate aerosols. Since the ice core estimates give us relatively accurate estimates of the hemispheric distribution of volcanic aerosols [*Gao et al.*, 2006], we can preserve this information by allowing transport only within the corresponding hemisphere. For eruptions without recorded month of eruption, we assumed that they occurred in April, as was done for the Volcanic Explosivity Index [*Simkin and Seibert*, 1994]. (The biases that may be introduced by this assumption are discussed in the next section.) Similar to the reconstruction of *Crowley* [2000] and *Ammann et al*. [2007], for eruptions without

recorded location we assumed a tropical eruption if there are signals in both Arctic and Antarctic ice cores, but a mid- to high-latitude eruption if signals were only found in one hemisphere.

To generate the time dependent data, we assume a linear buildup of the total aerosol mass for four months after eruption, leading to a maximum mass loading according to the strength of the eruption. After that we assume an exponential decrease of the stratospheric aerosol mass with a global mean e-folding time of 12 months. Since the major sink mechanism for stratospheric aerosol is stratosphere-troposphere folding in midlatitudes and the Brewer-Dobson circulation related sink in high latitudes [*Holton et al.*, 1995], we assume little loss due to sedimentation in the tropical regions (e-folding time of 36 months) and keep the sedimentation to an average e-folding time of 12 months in the extratropics. In the polar region, we set the e-folding time to be three months during winter to account for the strong subsidence in the polar vortex and six months for the rest of the year. By applying this latitude-season dependent function that describes the production and sedimentation of aerosols, we obtained a distribution of volcanic aerosols in latitude and time. Figure 5 shows an example of the resulting spatial and temporal distribution of the aerosol optical depth during the first three years after the Pinatubo eruption in 1991, where we see a linear increase of aerosol loading for the first four months and the seasonal transport to the poles. The result agrees fairly well with the satellite measurement and GCM calculations of Pinatubo optical depth [*Stenchikov et al.*, 1998]. Figure 6 shows the distribution for the 1809 Unknown and 1815 Tambora eruptions, where we can see not only the spread of volcanic aerosol in space and time but also the relative magnitude between the two eruptions. The total sulfate aerosol fluxes in the two polar regions after Tambora (47 kg/km^2 and 49 kg/km^2 in the Arctic and Antarctic respectively) and Pinatubo (13 kg/km^2 and 15 kg/km^2 in the Arctic and Antarctic respectively) are also in general agreement with the ice core observations (59 kg/km^2 and 51 kg/km^2 in Arctic and Antarctic respectively for Tambora, and 15

kg/km^2 for Pinatubo in the Antarctic), which serves as an important confirmation of the reliability of our transport and deposition program, despite its simplicity.

In the next step, we interpolated the vertical distribution of volcanic aerosols using information obtained from 11 lidar measurements of the aerosol backscattering coefficients at 0.525 μm wavelength after the 1991 Pinatubo eruption [*Antuña et al.*, 2002]. For each lidar dataset, we first calculated the total column backscattering coefficient for heights from 15 km to 30 km; then we calculated the ratios between backscattering coefficient for each 0.5 km depth and the total column value. This gives us the vertical distribution of Pinatubo aerosols in the stratosphere for the region. Based on visual inspection of radar measurements for the 1963 Agung eruption [*Grams and Fiocco*, 1967], ground lidar measurement for the 1974 Fuego eruption [*McCormick and Fuller*, 1975], and aircraft lidar measurement for the 1982 El Chichón eruption [*McCormick and Swissler*, 1983], the vertical distribution of volcanic aerosols have a similar shape in the stratosphere for these different eruptions, but peak at slightly different heights depending on the height of original ejection. Radiatively it does not make much of a difference in the climatic forcing. One could do sensitivity studies of this impact in a GCM, but that is beyond the scope of the present study here. Here we present "climatological" evolution of volcanic clouds.

Then we divided Earth into tropics (0-30°), midlatitudes (30-60°), high latitudes (60-70°), and polar region (70-90°), and calculated the regional mean vertical distribution of Pinatubo aerosol by averaging the lidar measurements in the corresponding regions. Finally we applied these four sets of vertical distribution functions to the monthly volcanic aerosol data we obtained above, assuming that each eruption has the same vertical distribution as Pinatubo in the corresponding regions. Figure 7 shows an example of the vertical distribution of volcanic aerosols six months after the Tambora eruption. We see that the center of sulfate aerosols

loading shifted from 18-25 km in the tropics to 14-20 km in the midlatitudes. The aerosols were more concentrated in the NH because it was in October and increasing planetary wave activity leading to isentropic mixing which enhanced the transport of aerosols into the winter hemisphere. This seasonal variation of wave activity is different between the two hemispheres due to different wave spectrum. The ice core sulfate data do not provide enough constraints to quantify this difference, and thus it is beyond the scope of this paper to include such difference into the reconstruction.

6. Uncertainties in the Reconstruction

Gao et al. [2007] listed uncertainties involved in using ice core records as a measure of the volcanic aerosol loading, and the improvements our method made in reducing these uncertainties. Nevertheless, there are still remaining uncertainties. We found spatial variation of about 50% for the 1815 Tambora deposition among both Arctic and Antarctica ice cores, and this number could be substantially larger for less well-known or less significant eruptions [*Gao et al.*, 2007]. Though our extensive body of ice core records, we significantly reduced the error associated with the estimations of the ice core volcanic sulfate deposition when compared to previous studies. The number of available ice cores constantly changes from one eruption to another and decreases dramatically for the early period. It is difficult to give a global quantitative estimate of the uncertainty related to the calculation of the ice core mean volcanic sulfate deposition. Further expansion of ice core availability in the future studies will help to reduce this uncertainty.

Besides the variation in the ice core deposition, there are uncertainties associated with the assumptions we made during the procedure to estimate the stratospheric aerosol loading, such as the choice of (1) twice the 31-year running median absolute deviation as the threshold to extract the volcanic signals (called 31pts+2MAD hereafter) and (2) April as the month of eruption. To

test the sensitivity to these assumptions in our reconstruction, we applied different choices of the above assumptions to the ice core records for the period from 1801 to 2000, keeping other procedures the same. The time frame was chosen because this is the period where we have the most ice core records and also several moderate to large volcanic events.

Uncertainty Associated with Different Signal Extraction Criteria and Calibration Factors

To estimate the sensitivity of the threshold and window length in the volcanic signal extraction procedure, we first changed the threshold to be 1.5MAD and 3MAD respectively while keeping the window length as 31-year; then we changed the window length to be 11-year, 51-year, and 101-year, respectively while keeping the threshold as 2MAD. This gives us six different sets of criteria including the original set. Applying these six sets of criteria to the ice core records for the past 200 years, we found that the different criteria do not significantly change either the detection of signals or their magnitude for moderate to larger volcanic eruptions (Figure 8). The 31pts+1.5MAD criterion picked up some additional signals as compared to the other methods. All of these additional signals are very small and we suspect that they are either false volcanic signals or not climatically significant. The El Chichón signal appears to be sensitive to the choice of the threshold (Fig. 8, upper panel) because most of our Arctic ice core records end before or around the 1980s and because the signals becomes more difficult to distinguish from the background toward the end. The El Chichón signal is missing from our Antarctic cores for almost all choices of criteria because of its very asymmetric hemispheric distribution, with almost all of the cloud staying in the NH [*Robock*, 2000]. The 11pts+2MAD criterion usually gave a lower estimate of sulfate loading for eruptions closely following another event, because it tends to filter out the decadal signal produced by consecutive eruptions as the background variation. Therefore, we disregard the 11pts+2MAD criterion from further calculation and discussion. The coefficient of variance among the five criteria is as

small as 4% for large eruptions like Tambora in 1815, and it increases to about 10% for moderate eruptions such as Krakatau in 1883 (Table 3). *Gao et al.* [2006] described why we chose 31pts+2MAD as our signal extraction criteria. Here we found that the estimated sulfate loading and the corresponding climate impacts are insensitive to the criteria chosen within a reasonable range, and the maximum uncertainty associated with the different choice of criteria is about 10%.

Uncertainty Associated with Eruptions Occurring in Different Seasons

The assumption of April as the time of eruption may introduce additional uncertainty because the seasonality of volcanic emission can affect its atmospheric transport and deposition in different latitudes. Since we were using a stratospheric transport parameterization to simulate the real work activity, we evaluated the uncertainty associated with this seasonality assumption in this parameterization program. In particular, we set the eruption time to be January, April, July and October representing winter, spring, summer, and fall (NH) eruptions, respectively, and ran the transport program with each setting. We assessed the difference in the high latitude volcanic sulfate deposition because this may reflect the uncertainty associated with our calculation of the total stratospheric aerosol loading using ice core records. Figure 9 plots the time series of sulfate deposition in the latitude band 60°-90° for each hemisphere. The major difference is the lag of deposition in time and how the signal is spread over multiple years. In terms of the total deposition, the difference among the four seasons is about 10%. A spring eruption distributed the least loading in NH high latitudes and the most in SH high latitudes among the four seasons, with the opposite for a fall eruption.

Figures 10 and 11 show the time series of Tambora sulfate aerosol loading in the midlatitudes and low latitudes for the four seasons. We found no significant differences (about 3% and 1% in extratropics and tropics, respectively) in the total loading. The major difference is again the lag of loading in time. In tropical regions, since the solar radiation is relatively

constant year around, this time lag in loading does not change the overall radiative affect; in mid-latitudes, however, this seasonal difference in peak loading may significantly change its overall radiative impact. For example, we found a large shift of sulfate aerosol loading from the first NH summer and fall to the following winter and spring in both hemispheres for a July and October eruption. As a result, we would expect the direct radiative (cooling) effect to be less in NH midlatitudes for a summer or fall eruption as compared to a spring eruption. In SH midlatitudes, the reduced cooling and increased warming later on balanced each other to some degree and we cannot predict the overall radiative effect based on our simple analysis. GCM simulations are necessary to test the detailed radiative, dynamic, and temperature responses associated with eruptions in different seasons, but it is beyond the scope of this paper.

According to the above comparison, the seasonality of eruption introduced another 10% uncertainty into our calculation of volcanic forcing time series. Nevertheless, the numerical distribution program is too simple to include some important climatic effects such as the QBO, and thus the seasonality difference may be larger than estimated here.

7. Conclusions

We have used 54 ice core records, 32 from the Arctic, including the 12 *Clausen and Hammer* ice cores and six PARCA cores, and 22 from Antarctica to generate a new volcanic forcing index for the past 1500 years. The index is a function of month from 501 to 2000, latitude in 10° bands, and height from 9 to 30 km at 0.5 km resolution. It is the longest and the most advanced volcanic forcing time series of this type, because it was based on the most comprehensive set of ice core records, plus an updated signal extraction method, ice-core-deposition to global stratospheric aerosol loading conversion factors, and a more advanced spatial-temporal transport parameterization scheme. Applying the global average volcanic forcing index together with solar and anthropogenic forcings to an upwelling diffusion

energy balance model we simulated the temperature response for the past 1500 years. The model results agree very well with both instrumental observations for the period 1850-2000 and the proxy reconstructions for the past millennium. With our volcanic forcing estimates, the model accurately simulated the cooling of about 0.2-0.3°C for three recent tropical eruptions, 1883 Krakatau, 1963 Agung, and 1991 Pinatubo eruption. The model simulated decadal temperature responses for the largest eruptions such as 1453 Kuwae and 1815 Tambora are also in good agreement with the proxy temperature reconstructions. The same index are being used in a coupled atmosphere-ocean GCM to better evaluate the climate change during the past millennium, and the results will be reported in a separate study.

By using 54 ice core records and accounting for the spatial variation of volcanic deposition in Greenland and Antarctic ice sheets, we significantly reduced the uncertainty in the new volcanic forcing index when compared to earlier studies. However, we still found a 4-10% uncertainty caused by different volcanic signal extraction criteria; 10% uncertainty in high-latitude sulfate deposition when assuming different eruption season in the transport program simulations, and on top of that a 25% uncertainty due to the choice of calibration factor. Nevertheless, this uncertainty range is much smaller than the factor of two uncertainty estimated in the early studies.

Time series of global and hemispheric total stratospheric sulfate injections from volcanic eruptions for the past 1500 years, as well as estimates of stratospheric loading as a function of latitude, altitude, and month (suitable for forcing GCMs) are available for downloading at http://climate.envsci.rutgers.edu/IVI2.html/.

Acknowledgments. We thank all the providers of the ice core data for their massive efforts in obtaining the ice cores, extracting the volcanic signals, and sharing the data with us. Without

their hard work, this study would not have been possible. We thank Jürgen Grieser for providing their diffusion sedimentation model and Tom Wigley for providing his climate model and both for help using the models. This work is supported by NOAA grant NA03-OAR-4310155.

References

Ammann, C. M., G. A. Meehl, W. M. Washington, and C .S. Zender (2003), A monthly and latitudinally varying volcanic forcing dataset in simulations of 20th century climate, *Geophys. Res. Lett.*, *30* (12), doi:10.1029/2003GL016875.

Ammann, C., F. Joos, D. S. Schimel, B. L. Otto-Bliesner, and R. A. Tomas (2007), Solar influence on climate during the past millennium: Results from transient simulations with the NCAR Climate System Model, *Proc. Nat. Acad. Sci.*, *104*, 3713-3718.

Antuña, J. C., A. Robock, G. L. Stenchikov, L. W. Thomason, and J. E. Barnes (2002), Lidar validation of SAGE II aerosol measurements after the 1991 Mount Pinatubo eruption, *J. Geophys. Res.*, *107* (D14), 4194, doi:10.1029/2001JD001441.

Bigler, M., D. Wagenbach, H. Fischer, J. Kipfstuhl, H. Millar, S. Sommer, and B. Stauffer (2002), Sulphate record from a northeast Greenland ice core over the last 1200 years based on continuous flow analysis, *Ann. Glaciol.*, *35*, 250-256.

Brönnimann, S., J. Luterbacher, J. Staeheli1, T. M. Svendby, G. Hansen, and T. Svenøe (2004), Extreme climate of the global troposphere and stratosphere in 1940–42 related to El Niño, *Nature*, *432*, 971-974.

Budner, D., and J. H. Cole-Dai (2003), The number and magnitude of large explosive volcanic eruptions between 904 and 1865 A.D.: quantitative evidence from a new south pole ice core, in *Volcanism and the Earth's Atmosphere*, edited by A. Robock, and C. Oppenheimer, pp. 165-176, AGU, Washington, D.C.

Castellano, E., S. Becagli, M. Hansson, M. Hutterli, J. R. Petit, M. R. Rampino, M. Severi, J. P. Steffensen, R. Traversi, and R. Udisti (2005), Holocene volcanic history as recorded in the

sulfate stratigraphy of the European Project for Ice Coring in Antarctica Dome C (EDC96) ice core, *J. Geophys. Res.*, *110*, D06114, doi:10.1029/2004JD005259.

Clausen, H. B., and C. U. Hammer (1988), The Laki and Tambora eruptions as revealed in Greenland ice cores from 11 locations, *Ann. Glacio.*, *10*, 16-22.

Cleveland, W. S. (1979), Robust locally weighted regression and smoothing scatterplots, *J. American Statistical Association*, *74*, 829-836.

Cleveland, W. S., and S. J. Devlin, (1988). Locally weighted regression: An approach to regression analysis by local fitting, *J. American Statistical Association*, *83*, 596-610.

Cole-Dai, J. H., E. Mosley-Thompson, and L. Thomason (1997), Annually resolved southern hemisphere volcanic history from two Antarctic ice cores, *J. Geophys. Res.*, *102*(D14), 16,761-16,771.

Cole-Dai, J. H., E. Mosley-Thompson, S. P. Wight, and L. Thomason (2000), A 4100-year record of explosive volcanism from an East Antarctica ice core, *J. Geophys. Res.*, *105*, 24,431-24,441.

Crowley, T. J. (2000), Causes of climate change over the past 1000 years, *Science*, *289*(5477), 270-277.

Crowley, T. J., and K. Y. Kim (1999), Modeling the temperature response to forced climate change over the last six centuries, *Geophys. Res. Lett.*, *26*(13), 1901-1904.

Delmas, R. J., S. Kirchner, J. M. Palais, and J. R. Petit (1992), 1000 years of explosive volcanism recorded at the South-Pole, *Tellus B*, *44* (4), 335-350.

Dixon, D., P. A. Mayewski, S. Kaspari, S. Sneed, and M. Handley (2004), A 200 year sub-annual record of sulfate in West Antarctica, from 16 ice cores, *Ann. Glaciol.*, *39*, 1-12.

Fisher, D. A., R. M. Koerner, and N. Reeh (1995), Holocene climatic records from Agassiz Ice Cap, Ellesmere Island, NWT, Canada, *Holocene*, *5*(1), 19-24.

Gao, C., L. Oman, A. Robock, and G. L. Stenchikov (2007), Atmospheric volcanic loading derived from bipolar ice cores accounting for the spatial distribution of volcanic deposition, *J. Geophys. Res.*, *112*, D09109, doi:10.1029/2006JD007461.

Gao, C., A. Robock, S. Self, J. B. Witter, J. P. Steffenson, H. B. Clausen, M. L. Siggaard-Andersen, S. Johnsen, P. A. Mayewski, and C. Ammann (2006), The 1452 or 1453 AD Kuwae eruption signal derived from multiple ice core records: Greatest volcanic sulfate event of the past 700 years, *J. Geophys. Res.*, *111*(D12), doi:10.1029/2005JD006710.

Gilliland, R., and S. Schneider (1984), Volcanic, CO_2 and solar forcings of Northern and Southern Hemisphere surface air temperatures, *Nature*, *310*, 38-41.

Grams, G. and G. Fiocco (1967), Stratospheric aerosol layer during 1964 and 1965, *J. Geophys. Res.*, *72*, 3523-3542.

Graf, H.-F., Q. Li, and M. A. Giorgetta (2007), Volcanic effects on climate: revisiting the mechanisms, *Atmos. Chem. Phys.*, *7*(17), 4503-4511.

Grieser, J., and C. D. Schönwiese (1999), Parameterization of spatio-temporal patterns of volcanic aerosol induced stratospheric optical depth and its climate radiative forcing, *Atmosféra*, *12*(2), 111-133.

Hammer, C. U. (1977), Past volcanism revealed by Greenland ice sheet impurities, *Nature*, *270* (5637), 482-486.

Hammer, C. U. (1980), Acidity of polar ice cores in relation to absolute dating, past volcanism, and radio echoes, *J. Glaciol.*, *25*(93), 359-372.

Holton, J. R., P. H. Haynes, M. E. Mcintyre, A. R. Douglass, R. B. Rood, and L. Pfister (1995), Stratosphere-troposphere exchange, *Rev. Geophys.*, *33*, 403-439.

IPCC (2007), *Climate Change 2007: The Physical Science Basis. Contribution of Working Group I to the Fourth Assessment Report of the Intergovernmental Panel on Climate Change*,

S. Solomon, D. Qin, M. Manning, Z. Chen, M. Marquis, K. B. Averyt, M. Tignor and H. L. Miller, eds., (Cambridge University Press, Cambridge, United Kingdom and New York, NY, USA), 996 pp.

Kurbatov, A. V., G. A. Zielinski, N. W. Dunbar, P. A. Mayewski, E. A. Meyerson, S. B. Sneed, and K. C. Taylor (2006), A 12,000 year record of explosive volcanism in the Siple Dome Ice Core, West Antarctica, *J. Geophys. Res.*, *111*, D12307, doi:10.1029/2005JD006072.

Lamb, H. H. (1970), Volcanic dust in the atmosphere, with a chronology and assessment of its meteorological significace, *Philos. Trans. R. Soc. London*, *266* (A), 425-533.

Langway, C. C., K. Osada, H. B. Clausen, C. U. Hammer, and H. Shoji (1995), A 10-century comparison of prominent bipolar volcanic events in ice cores, *J. Geophys. Res.*, *100*, 16,241-16,247.

Legrand, M., and R. Delmas (1987), A 220 year continuous record of volcanic H_2SO_4 in the Antarctic ice sheet, *Nature*, *327*, 671-676.

Mayewski, P. A., W. B. Lyons, M. J. Spencer, M. S. Twickler, C. F. Buck, and S. Whitlow (1990), An ice-core record of atmospheric response to anthropogenic sulfate and nitrate, *Nature*, *346* (6284), 554-556.

McCormick, M. P., and W. H. Fuller, Jr. (1975), Lidar measurements of two intense stratospheric dust layers, *Appl. Opt.*, *14*, 4-13.

McCormick, M. P., and T. J. Swissler (1983), Stratospheric aerosol mass and latitudinal distribution of the El Chichón eruption cloud for October 1982, *Geophys. Res. Lett.*, *10*, 877-880.

Mitchell, J. M., Jr.(1970) A preliminary evaluation of atmospheric pollution as a cause of the global temperature fluctuation of the past century, in *Global Effects of Environmental Pollution*, edited by S. F. Singer, pp. 139-155, D. Reidel.

Moore, J. C., H. Narita, and N. Maeno (1991), A continuous 770-year record of volcanic activity from East Antarctica, *J. Geophys. Res*., *96*(D9), 17,353-17,359.

Mosley-Thompson, E., T. A. Mashiotta, and L. Thompson (2003), High resolution ice core records of late Holocene volcanism: Current and future contributions from the Greenland PARCA cores, in *Volcanism and the Earth's Atmosphere*, edited by A. Robock, and C. Oppenheimer, pp. 153-164, American Geophysical Union, Washington, D.C.

Mosley-Thompson, E., L. G. Thompson, J. Dai, M. Davis, and P. N. Lin (1993), Climate of the last 500 years: High-resolution ice core records, *Quaternary Sci. Rev.*, *12*(6), 419-430.

Muscheler, R., F. Joos, J. Beer, S. A. Muller, M. Vonmoos, and I. Snowball (2007), Solar activity during the last 1000 yr inferred from radionuclide records, *Quaternary. Sci. Rev.*, *26*(1-2), 82-97.

Newhall, C. G., and S. Self (1982), The volcanic explosivity index (VEI): An estimate of explosive magnitude for historical volcanism, *J. Geophys. Res*., *87*, 1231-1238.

Palmer, A. S., V. I. Morgan, A. J. Curran, T. D. Van Ommen, and P. A. Mayewski (2002), Antarctic volcanic flux ratios from Law Dome ice cores, *Ann. Glaciol.*, *35*, 329-332.

Pinto, J.P., R.P. Turco, and O.B. Toon (1989), Self-limiting physical and chemical effects in volcanic eruption clouds, *J. Geophys. Res.*, *94*, 11,165-11,174.

Robertson, A., J. Overpeck, D. Rind, E. Mosley-Thompson, G. Zielinski, J. Lean, D. Koch, J. Penner, I. Tegen, and R. Healy (2001), Hypothesized climate forcing time series for the last 500 years, *J. Geophys. Res*., *106* (D14), 14,783-14,803.

Robock, Alan (1981), A latitudinally dependent volcanic dust veil index, and its effect on climate simulations, *J. Volcanol. Geotherm. Res.*, *11*, 67-80.

Robock, A. (2000), Volcanic eruptions and climate, *Rev. Geophys.*, *38*, 191-219.

Robock, A (2005), Cooling following large volcanic eruptions corrected for the effect of diffuse radiation on tree rings. *Geophys. Res. Lett.*, 32, L06702, doi:10.1029/2004GL022116.

Robock, A., and M. P. Free (1995), Ice cores as an index of global volcanism from 1850 to the present, *J. Geophys. Res.*, *100* (D6), 11,549-11,567.

Robock, A., and M. Free (1996), The volcanic record in ice cores for the past 2000 years, in *Climatic Variations and Forcing Mechanisms of the Last 2000 Years*, edited by P. Jones, R. Bradley, and J. Jouzel, pp. 533-546, Springer-Verlag, Berlin.

Robock, A. and J. Mao (1992), Winter warming from large volcanic eruptions, *Geophys. Res. Lett.*, *19*, 2405-2408.

Sato, M., J. E. Hansen, M. P. McCormick, and J. B. Pollack (1993), Stratospheric aerosol optical depths, 1850-1990, *J. Geophys. Res.*, *98*(D12), 22,987-22,994.

Simkin, T., and L. Siebert (1994), *Volcanoes of the World*, 349 pp., Geoscience Press, Tucson, Az.

Sommer, S., C. Appenzeller, R. Rothlisberger, M. Hutterli, B. Stauffer, D. Wagenbach, H. Oerter, F. Wilhelms, D. J. Miller, and R. Mulvaney (2000), Glacio-chemical study spanning the past 2 kyr on three ice cores from Dronning Maud Land, Antarctica 1. Annually resolved accumulation rates, *J. Geophys. Res.*, *105* (D24), 29,411-29,421.

Stenchikov, G. L., I. Kirchner, A. Robock, H.-F. Graf, J. C. Antuña, R. G. Grainger, A. Lambert, and L. Thomason (1998), Radiative forcing from the 1991 Mount Pinatubo volcanic eruption. *J. Geophys. Res.*, *103*, 13,837-13,857.

Stenchikov, G., A. Robock, V. Ramaswamy, M. D. Schwarzkopf, K. Hamilton, and S. Ramachandran (2002), Arctic Oscillation response to the 1991 Mount Pinatubo eruption: Effects of volcanic aerosols and ozone depletion, *J. Geophys. Res.*, *107*(D24), 4803, doi:10.1029/2002JD002090.

Stenni, B., M. Proposito, R. Gragnani, O. Flora, J. Jouzel, S. Falourd, and M. Frezzotti (2002), Eight centuries of volcanic signal and climate change at Talos Dome (East Antarctica), *J. Geophys. Res.*, *107*(D9), doi:10.1029/2000JD000317.

Stothers, R. B. (1984), The Great Tambora Eruption in 1815 and its aftermath, *Science*, *224* (4654), 1191-1198.

Stothers, R. B. (1996), Major optical depth perturbations to the stratosphere from volcanic eruptions: Pyrheliometric period, 1881-1960, *J. Geophys. Res.*, *101* (D2), 3901-3920.

Stothers, R. B. (2001), Major optical depth perturbations to the stratosphere from volcanic eruptions: Stellar extinction period, 1961-1978, *J. Geophys. Res.*, *106* (D3), 2993-3003.

Thompson, D. W. J., J. J. Kennedy, J. M. Wallace, P. D. Jones (2008), A large discontinuity in the mid-twentieth century in observed global-mean surface temperature, *Nature*, *453*, 646-649, doi:10.1038/nature06982.

Toon, O. B., and J. B. Pollack (1980), Atmospheric aerosols and climate, *Am. Sci.*, *68*, 268-278.

Traufetter, F., H. Oerter, H. Fischer, R. Weller, and H. Miller (2004), Spatio-temporal variability in volcanic sulphate deposition over the past 2kyr in snow pits and firn cores from Amundsenisen, Antarctica, *J. Glaciol.*, *50*, 137-146.

Wang, Y. M., J. L. Lean, and N. R. Sheeley (2005), Modeling the sun's magnetic field and irradiance since 1713, *Astrophysical Journal*, *625*(1), 522-538.

Wigley, T. M. L., and S. C. B. Raper (1992), Implications for climate and sea-level of revised IPCC emissions scenarios, *Nature*, *357*(6376), 293-300.

Wigley, T. M. L., and S. C. B. Raper (2001), Interpretation of high projections for global-mean warming, *Science*, *293*(5529), 451-454.

Wigley, T. M. L., C. M. Ammann, B. D. Santer, and S. C. B. Raper (2005), Effect of climate sensitivity on the response to volcanic forcing, *J. Geophys. Res*, *110*(D09107), doi:10.1029/2004JD005557.

Zielinski, G. A. (1995), Stratospheric loading and optical depth estimates of explosive volcanism over the last 2100 years derived from the Greenland-Ice-Sheet-Project-2 ice core, *J. Geophys. Res.*, *100*(D10), 20,937-20,955.

Zielinski, G. A., M. S. Germani, G. Larsen, M. G. L. Baillie, S. Whitlow, M. S. Twickler, and K. Taylor (1995), Evidence of the Eldgja (Iceland) eruption in the GISP2 Greenland ice core - relationship to eruption processes and climatic conditions in the 10th-century, *Holocene*, *5*(2), 129-140.

Table 1. Ice core time series used in the study. Ice cores marked with * are ones used by [*Robock and Free*, 1995]. ECM = electrical conductivity measurement, DEP=dielectric profiling, NSS SO4=non-sea-salt sulfate, CFA=continuous flow analysis, NSS-conductivity=non-sea-salt conductivity, EXS=excess sulfate.

Name	Location	Period	Resolution	Measure Type	Units	Reference
A84*	80.7ºN, 73.1ºW	1223-1961	1/a	ECM	µA	*Fisher et al.* [1995]
A77*	80.7ºN, 73.1ºW	453-1853	1/a	ECM	µA	*Fisher et al.* [1995]
NGT_B20	79ºN, 36.5ºW	830-1993	12/a	CFA	ng/g (ppb)	*Bigler et al.* [2002]
NorthGRIP1.ECM	75.1ºN, 42.3ºW	190-1969	2/a	ECM		*Gao et al.* [2006]
NorthGRIP1.SO_4	75.1ºN, 42.3ºW	190-1969	1/a	Total SO_4	µequiv/kg	*Gao et al.* [2006]
GISP2*	72.6ºN, 38.5ºW	1-1984	0.5/a	NSS SO_4	ppb	*Zielinski* [1995]
Dye3 deep	72.6ºN, 37.6ºW	1-1768	4/a	ECM		*Gao et al.* [2006]
Greenland Site T	72.6ºN,38.5 W	1731-1989	1/a	EXS	kg/km^2	*Mosley-Thompson et al.* [1993]
GRIP main	71.3ºN, 26.7ºW	1-1642	4/a	ECM		*Gao et al.* [2006]
Crête	71.1ºN, 37.3ºW	553-1778	4/a	ECM		*Gao et al.* [2006]
Greenland Site A	70.8ºN, 36°W	1715-1985	1/a	EXS	kg/km^2	*Mosley-Thompson et al.* [1993]
Renland	70.6ºN, 35.8ºW	1000-1984	1/a	ECM		*Gao et al.* [2006]
20D*	65ºN, 45ºW	1767-1983	1/a	NSS SO_4	ng/g	*Mayewski et al.* [1990]
Mt. Logan*	60.6ºN, 141ºW	1689-1979	1/a	total SO_4	µequiv/l	*Mayewski et al.* [1990]
Law Dome	66.7ºS 112.8ºE	1301-1995	12/a	NSS SO_4	µequiv/l	*Palmer et al.* [2002]
Dyer	70.7ºS, 65ºW	1505-1989	1/a	total SO_4 flux	kg/km^2	*Cole-Dai et al.* [1997]
G15*	71.2ºS, 46ºE	1210-1983	varies	DEP	µS/m	*Moore et al.* [1991]
Talos Dome	72.8ºS, 159.1ºE	1217-1996	varies	NSS SO_4	µequiv/l	*Stenni et al.* [2002]
Hercules Névé	73.1ºS, 165.5ºE	1774-1992	1/a	NSS SO_4	µequiv/l	*Stenni et al.* [2002]
Dome C*	74.7ºS, 124.2ºE	1763-1973	1/a	NSS SO_4	µequiv./l	*Legrand and Delmas* [1987]
DML_B32.SO_4	75ºS, 0ºW	159-1997	varies	NSS SO_4	ng/g	*Traufetter et al.* [2004]
DML_B32.ECM	75ºS, 0ºW	159-1997	12/a	NSS-conductivity	µS/cm	*Sommer et al.* [2000]
DML_B33	75.2ºS, 6.5ºW	1-1996	12/a	NSS-conductivity	µS/cm	*Sommer et al.* [2000]
DML_B31	75.6ºS, 3.5ºW	463-1994	12/a	NSS-conductivity	µS/cm	*Sommer et al.* [2000]
Siple Station	76ºS, 84.3ºW	1417-1983	1/a	Total SO_4 flux	kg/km^2	*Cole-Dai et al.* [1997]
ITASE 01-5	77ºS, 89ºW	1781-2002	varies	SO_4	µg/l	*Dixon et al.* [2004]
ITASE 00-5	77.7ºS, 124ºW	1708-2001	varies	SO_4	µg/l	*Dixon et al.* [2004]
ITASE 00-4	78ºS, 120ºW	1799-2001	varies	SO_4	µg/l	*Dixon et al.* [2004]
ITASE 01-3	78.1ºS, 95.6ºW	1859-2002	varies	SO_4	µg/l	*Dixon et al.* [2004]
ITASE 00-1	79.4ºS, 111ºW	1651-2001	varies	SO_4	µg/l	*Dixon et al.* [2004]
ITASE 99-1	80.6ºS,122.6ºW	1713-2000	varies	SO_4	µg/l	*Dixon et al.* [2004]
Plateau Remote*	84ºS, 43ºE	1-1986	1/a	SO_4	ppb	*Cole-Dai et al.* [2000]
PS1*	90ºS	1010-1984	1/a	NSS SO_4	ng/g	*Delmas et al.* [1992]
PS14*	90ºS	1800 - 1984	1/a	NSS SO_4	ng/g	*Delmas et al.* [1992]
SP2001c1	90ºS	905-1999	1/a	Total SO_4 flux	kg/km^2	*Budner and Cole-Dai* [2003]
SP95	90ºS	1487-1992	varies	SO_4	µg/l	*Dixon et al.* [2004]

Table 2. Exchange coefficients for different regions in percentage (%) per month. Original values from *Grieser and Schönwiese* [1999].

Regions	Original Values	Values in this paper
tropics → tropics	91	91
tropics → extratropics	30	50
extratropics → tropics	7	7
extratropics ↔ extratropics (winter-spring)	90	90
extratropics ↔ extratropics (summer-fall)	45	70
extratropics → winter polar vortex	10	10
extratropics → summer polar region	45	70
extratropics → polar region in spring and fall	28	40
polar region→ extratropics	10/45/28	4

Table 3. Total sulfate deposition from different volcanic signal extraction criteria.

Eruption	31pts+2MAD (Tg)	31pts+1.5MAD (Tg)	31pts+3MAD (Tg)	11pts+2MAD (Tg)	51pts+2MAD (Tg)	101pts+2MAD (Tg)	s.d.* (Tg)	Cvar* (%)
1809 Unknown	58.7	62.4	55.6	57.3	61.7	65.2	3.36	5.6
1815 Tambora	120	121	117	101	125	129	4.53	3.7
1831 Unknown	17.0	17.2	18.7	13.1	16.7	14.8	1.42	8.4
1835 Cosigüina	40.2	39.4	37.7	25.2	37.1	36.8	1.48	3.9
1883 Krakatau	26.9	27.8	22.5	21.1	26.2	22.1	2.63	10.5
1912 Katmai	22.0	22.3	21.1	19.3	22.9	25.4	1.61	7.1
1991 Pinatubo	30.1	30.3	20.0	7.2	27.6	30.2	4.40	15.9

* Standard deviation (s.d.) and coefficient of variance (Cvar) were calculated using the five sets of extraction criteria, leaving out the 11pts+2MAD criterion (see text).

Figure Captions

Figure 1. Distribution of ice core sites in the Arctic and Antarctic. See Table 1 for details about each time series.

Figure 2. Annual stratospheric volcanic sulfate aerosol injection for the past 1500 years in the NH (top), SH (middle), and global (bottom).

Figure 3. Global average surface air temperature anomalies, with respect to the 1961-1990 mean, simulated with the *Wigley and Raper* [1992, 2001] upwelling-diffusion energy balance model (MAGICC) and observed data (from the Climatic Research Unit http://www.cru.uea.ac.uk/cru/data/temperature/).

Figure 4. MAGICC simulated NH temperature response (red curve) plotted on top of temperature reconstructions (shaded) and instrumental observations (black curve) [*IPCC*, 2007, Fig 6.10, used with permission]. We plotted smoothed (31-year running mean) temperature anomalies with respect to the 1961-1990 mean.

Figure 5. Distribution of total aerosol optical depth for the 1991 Pinatubo eruption from our data set.

Figure 6. Distribution of sulfate aerosol loading from the 1809 Unknown and 1815 Tambora eruptions. By comparison, the maximum tropical loading for the 1991 Pinatubo eruption was 132 kg/km^2.

Figure 7. Latitude-altitude distribution of sulfate aerosol loading for Oct. 1815, six months after the Tambora eruption.

Figure 8. Comparison of global sulfate aerosol loading calculated using different signal extraction criteria.

Figure 9. High latitude sulfate deposition for the Tambora eruption, assuming eruptions at different times of the year. L_t is the average sulfate aerosol loading in each latitude band. NH high latitude is 61°N-90°N and SH high latitude is 61°S-90°S.

Figure 10. Midlatitude sulfate loading for the Tambora eruption, assuming eruptions at different times of the year. L_t is the average sulfate aerosol loading in each latitude band. NH midlatitude is 22°N-61°N and SH midlatitude is 22°S-61°S.

Figure 11. Low latitude sulfate loading for the Tambora eruption, assuming eruptions at different times of the year. L_t is the average sulfate aerosol loading in each latitude band. NH low latitude is 0°-22°N and SH low latitude is 0°-22°S.

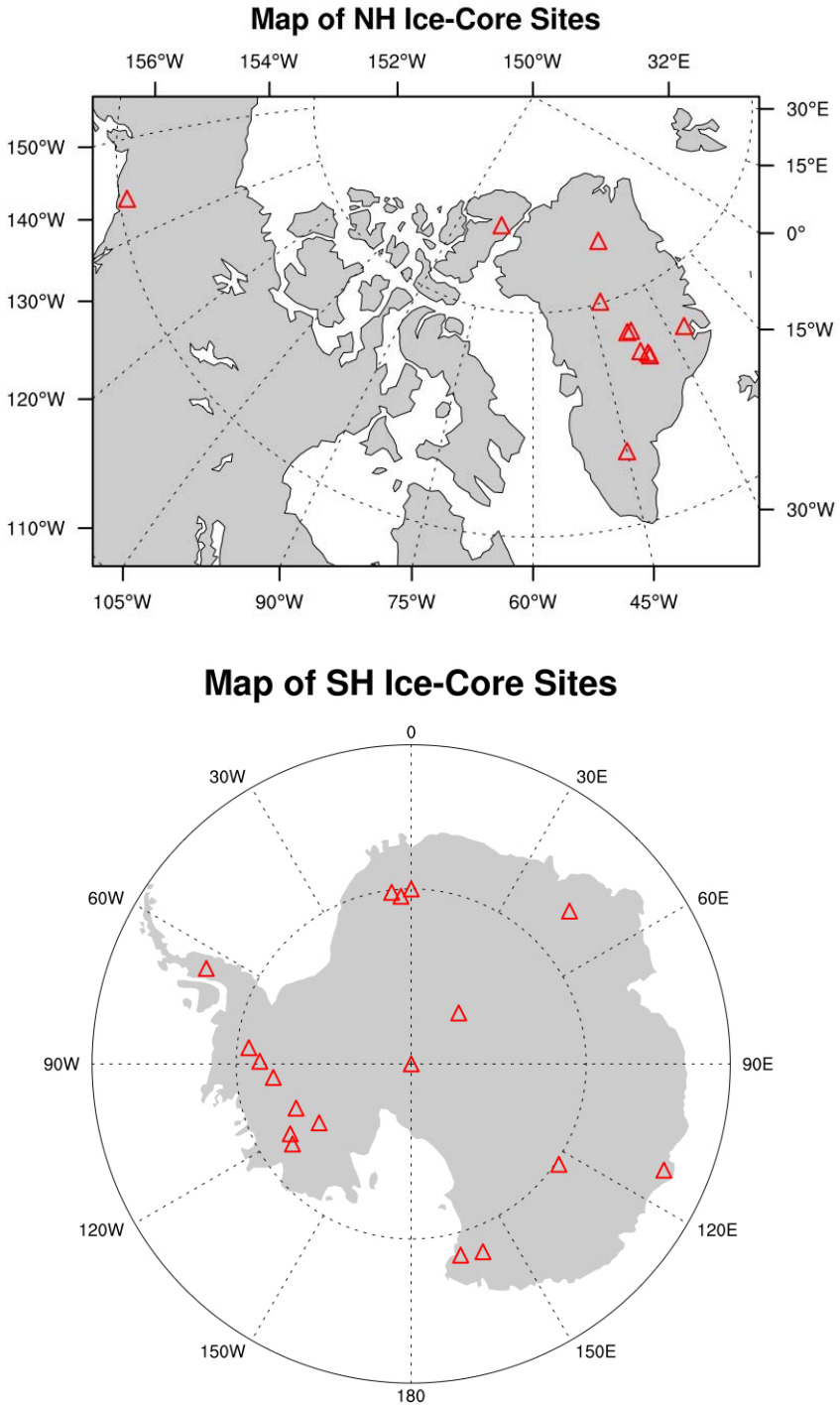

Figure 1. Distribution of ice core sites in the Arctic and Antarctic. See Table 1 for details about each time series.

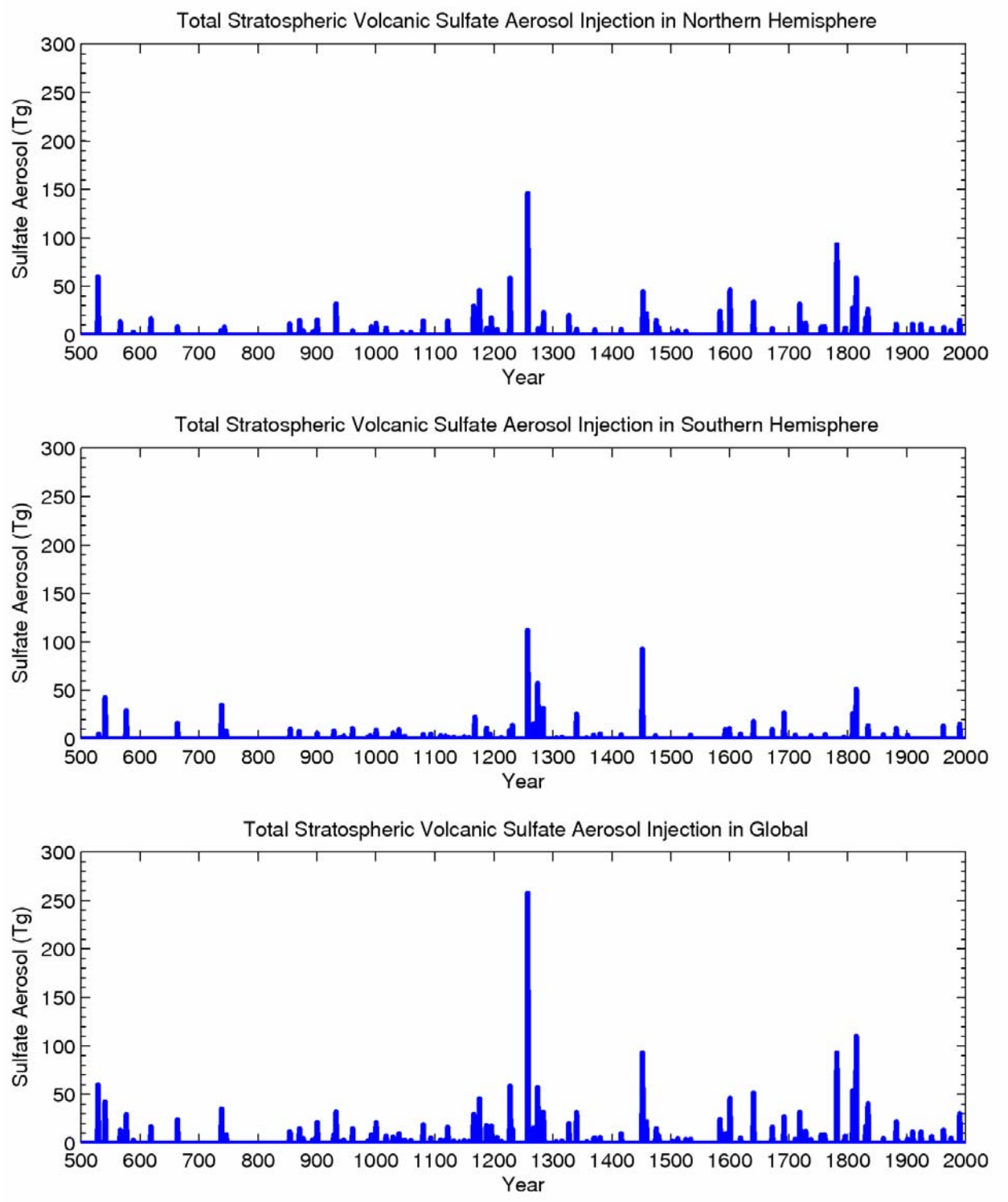

Figure 2: Annual stratospheric volcanic sulfate aerosol injection for the past 1500 years in the NH (up), SH (middle), and global (bottom).

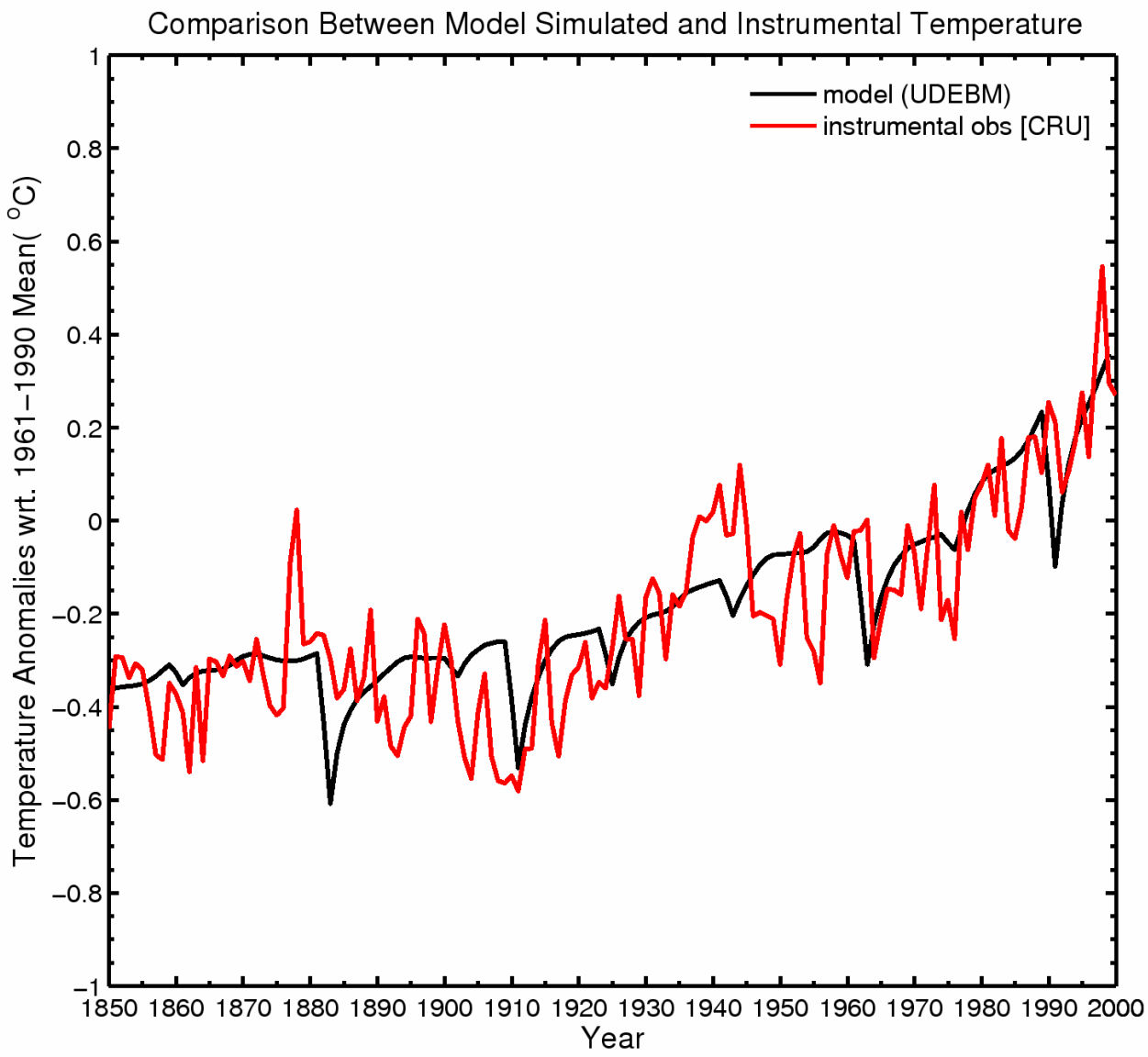

Figure 3. Global average surface air temperature anomalies, with respect to the 1961-1990 mean, simulated with the *Wigley and Raper* [1992, 2001] upwelling-diffusion energy balance model (MAGICC) and observed data (from the Climatic Research Unit http://www.cru.uea.ac.uk/cru/data/temperature/).

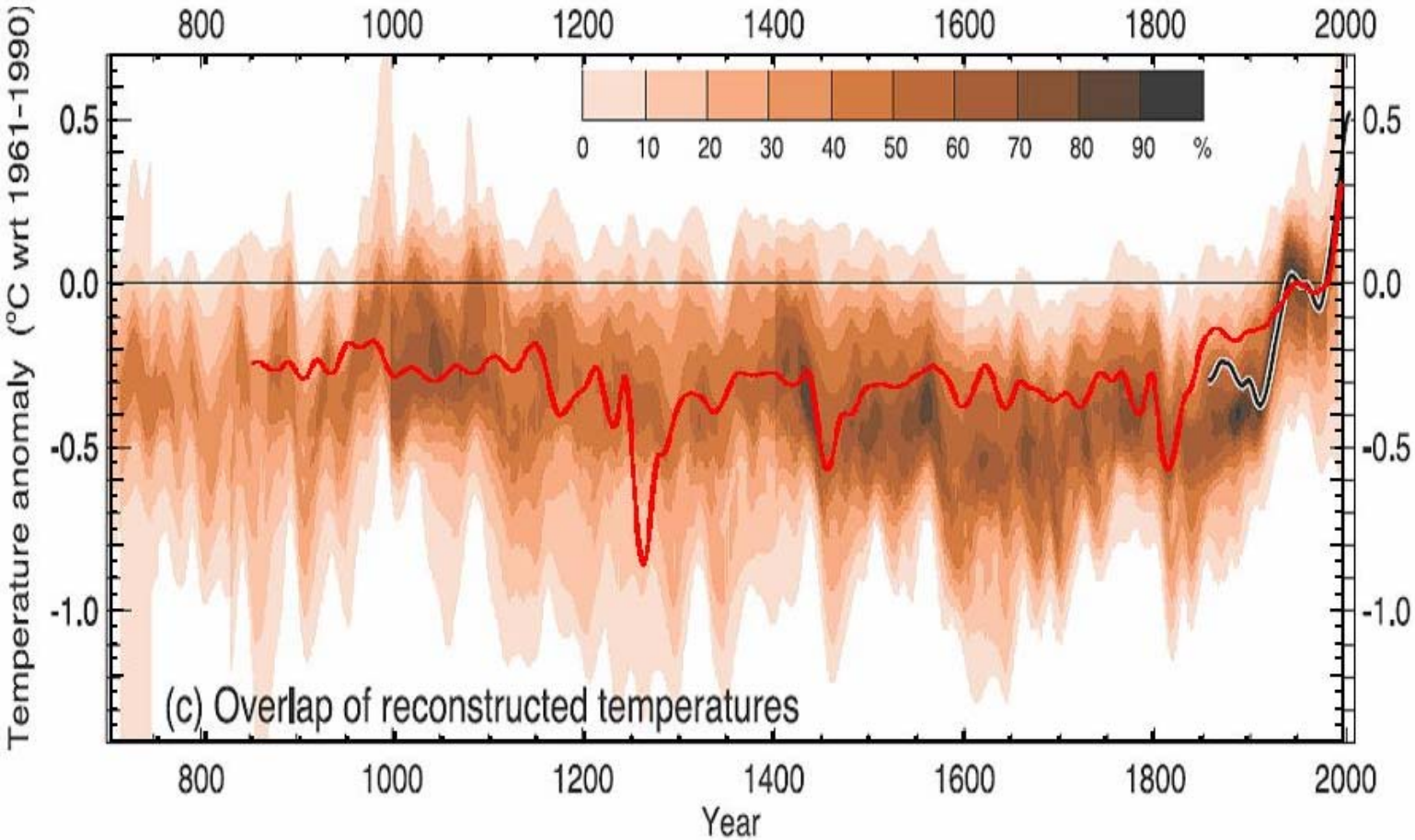

Figure 4. MAGICC- simulated NH temperature response (red curve) plotted on top of temperature reconstructions (shaded) and instrumental observations (black curve) [*IPCC*, 2007, Fig 6.10, used with permission]. We plotted smoothed (31-year weighted mean) temperature anomalies with respect to the 1961-1990 mean.

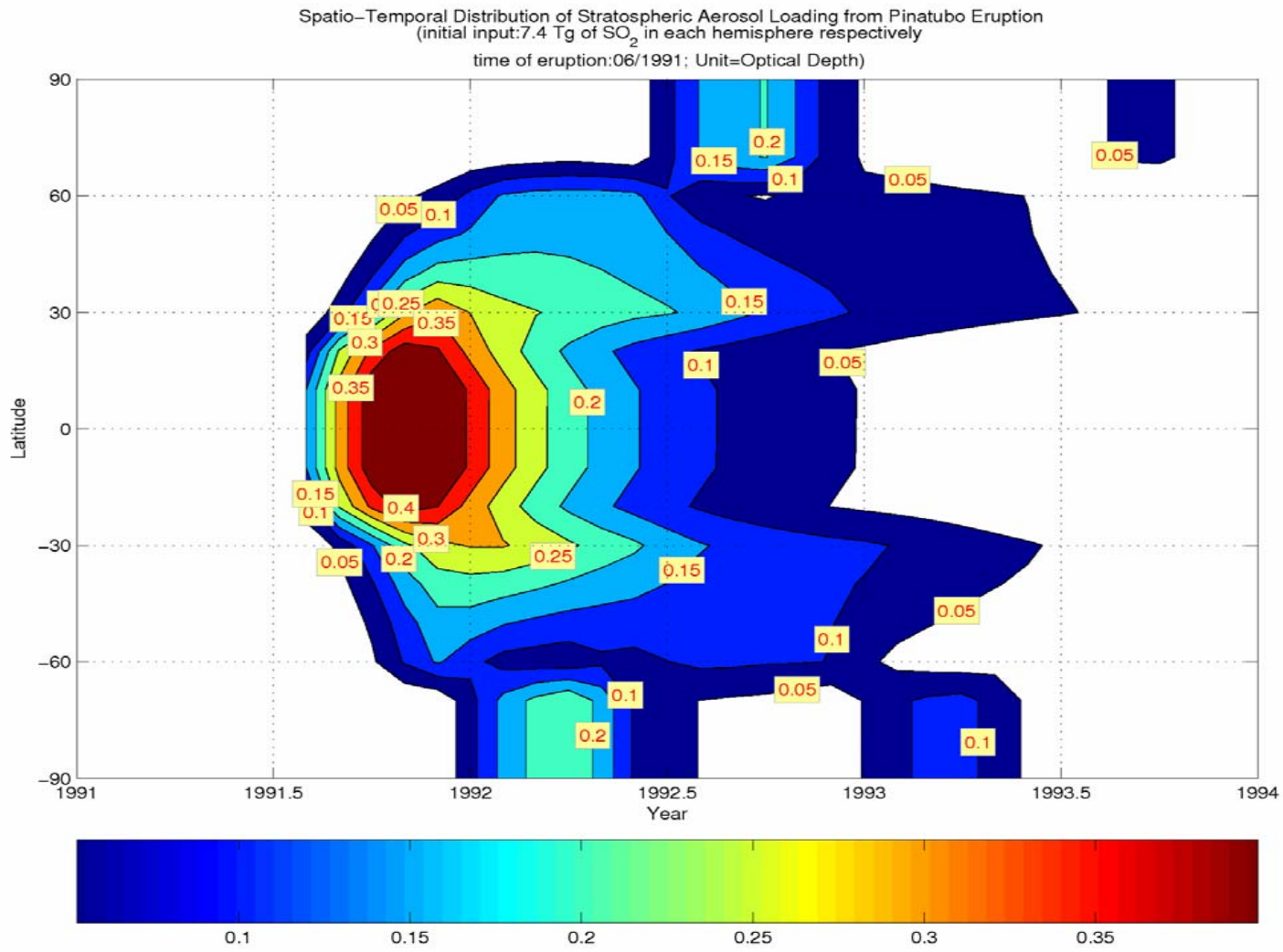

Figure 5. Distribution of total aerosol optical depth for the 1991 Pinatubo eruption from our data set.

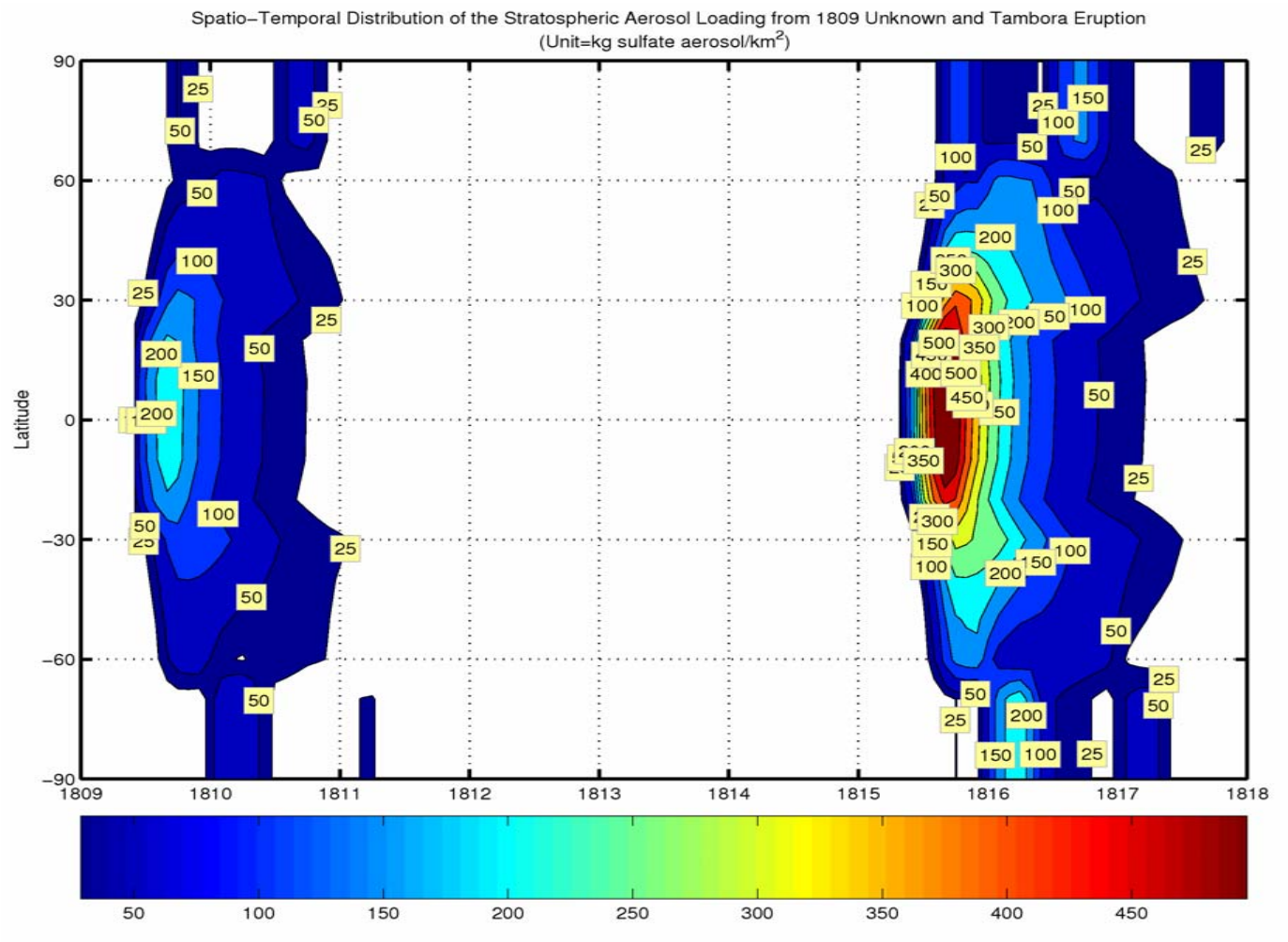

Figure 6. Distribution of sulfate aerosol loading from 1809 Unknown and 1815 Tambora eruptions. By comparison, the maximum tropical loading for the 1991 Pinatubo eruption was 132 kg/km^2.

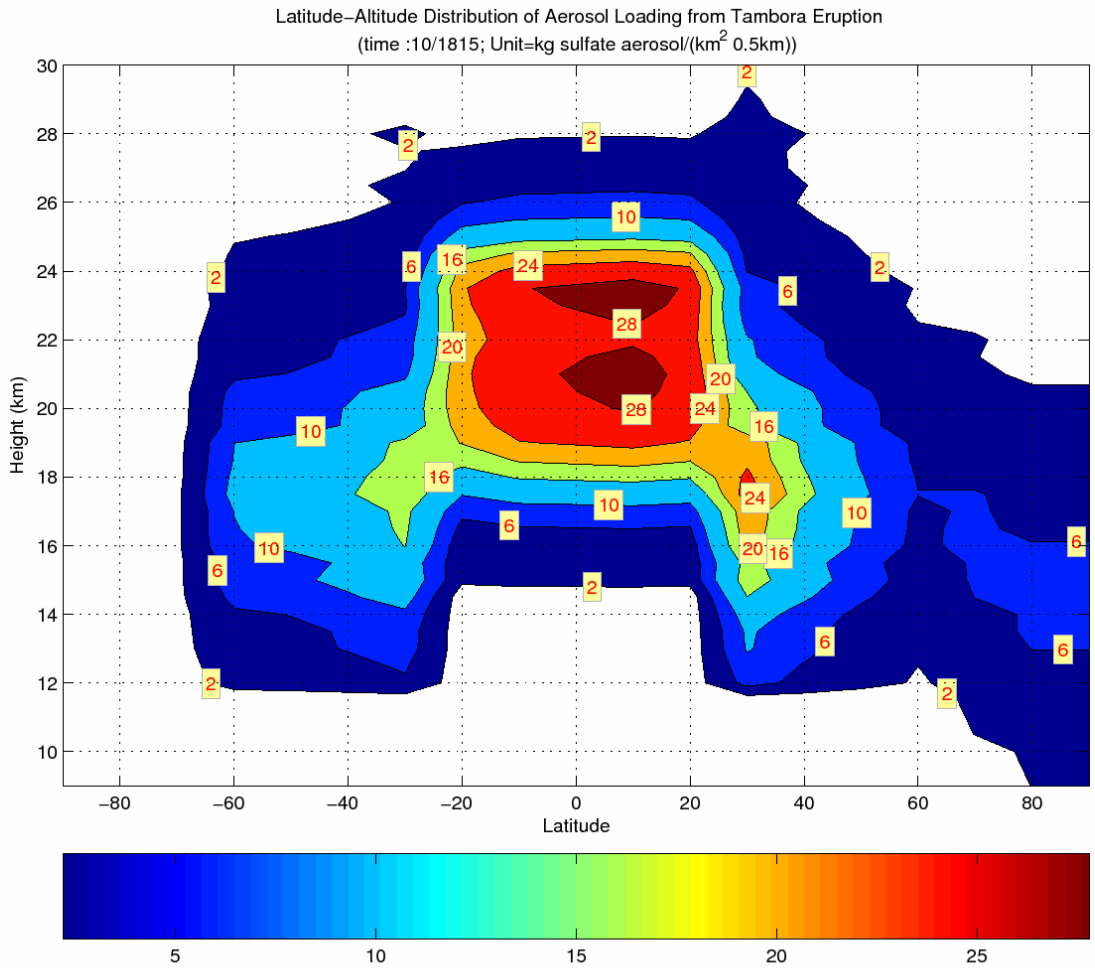

Figure 7. Latitude-altitude distribution of sulfate aerosol loading for Oct. 1815, six months after the Tambora eruption.

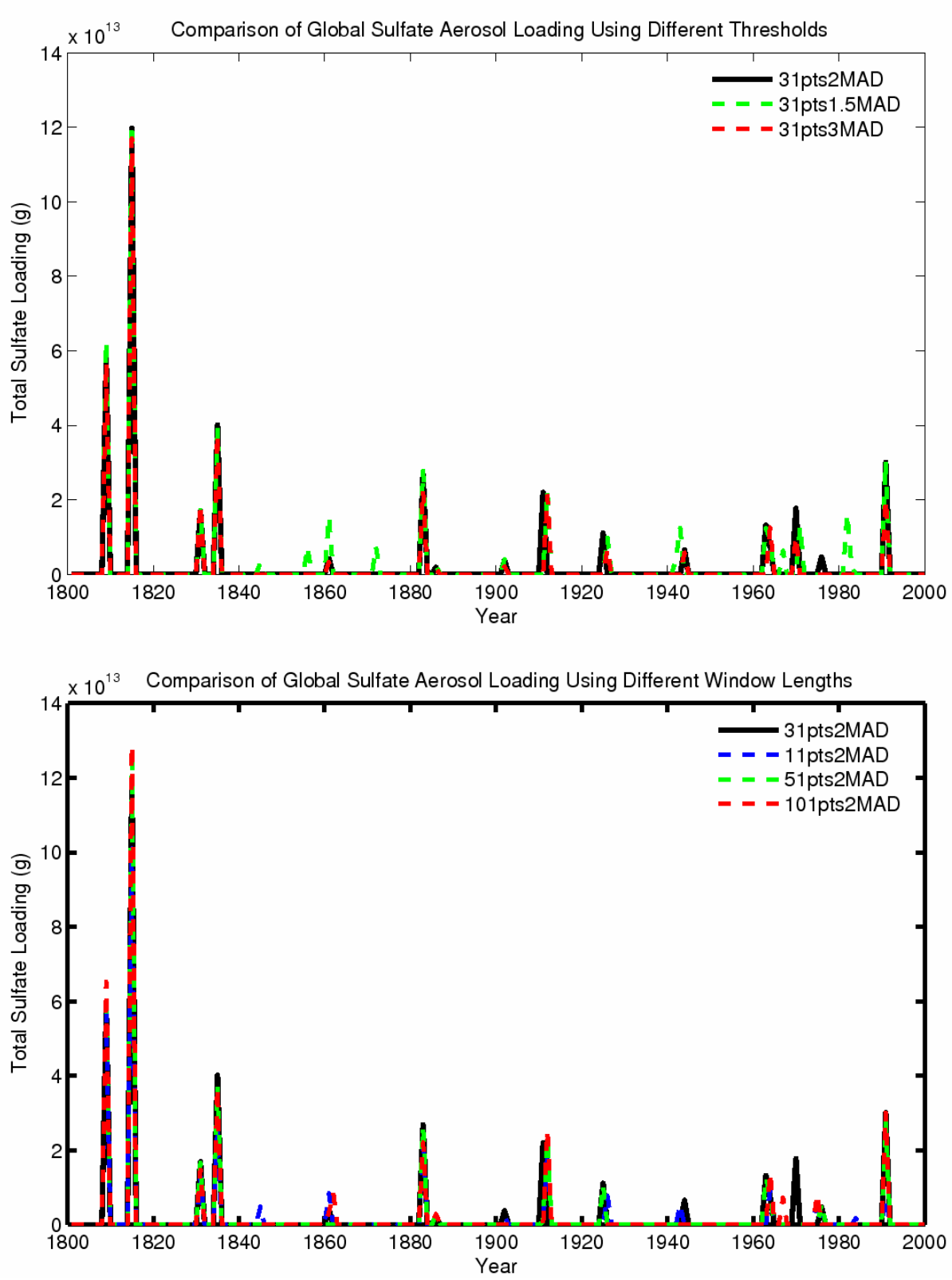

Figure 8. Comparison of global sulfate aerosol loading calculated using different signal extraction criteria.

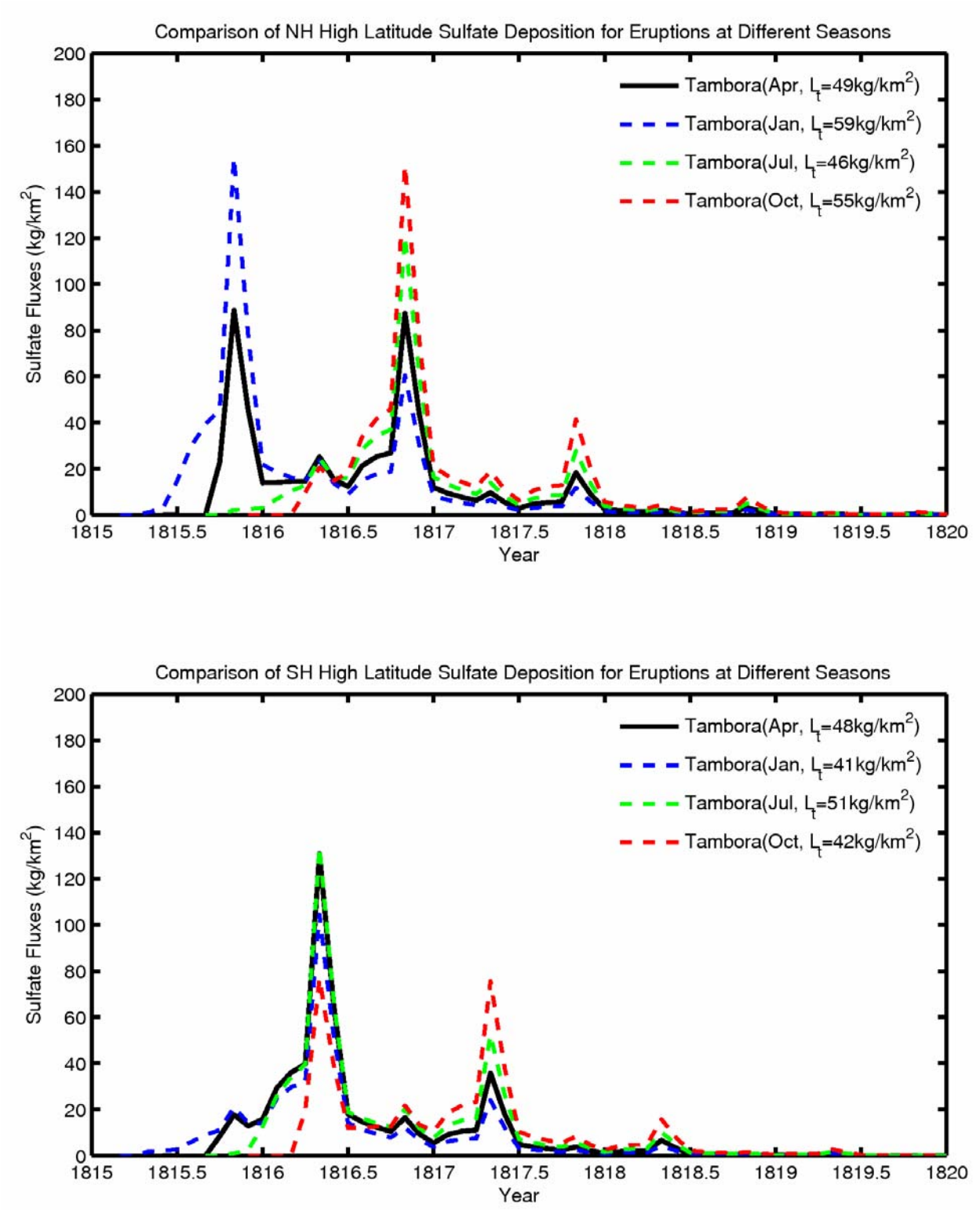

Figure 9. High latitude sulfate deposition for the Tambora eruption, assuming eruptions at different times of the year.

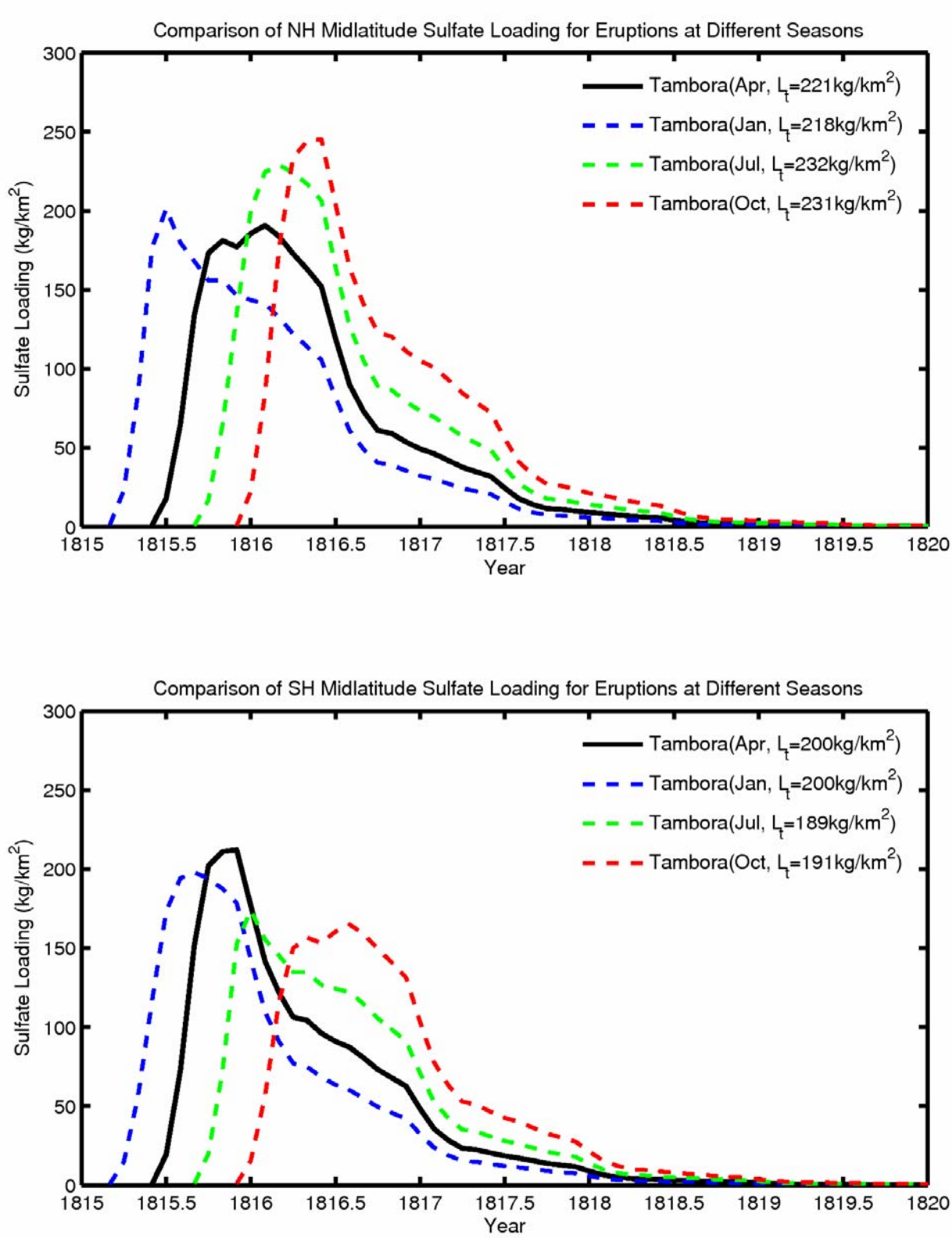

Figure 10. Midlatitude sulfate loading for the Tambora eruption, assuming eruptions at different times of the year.

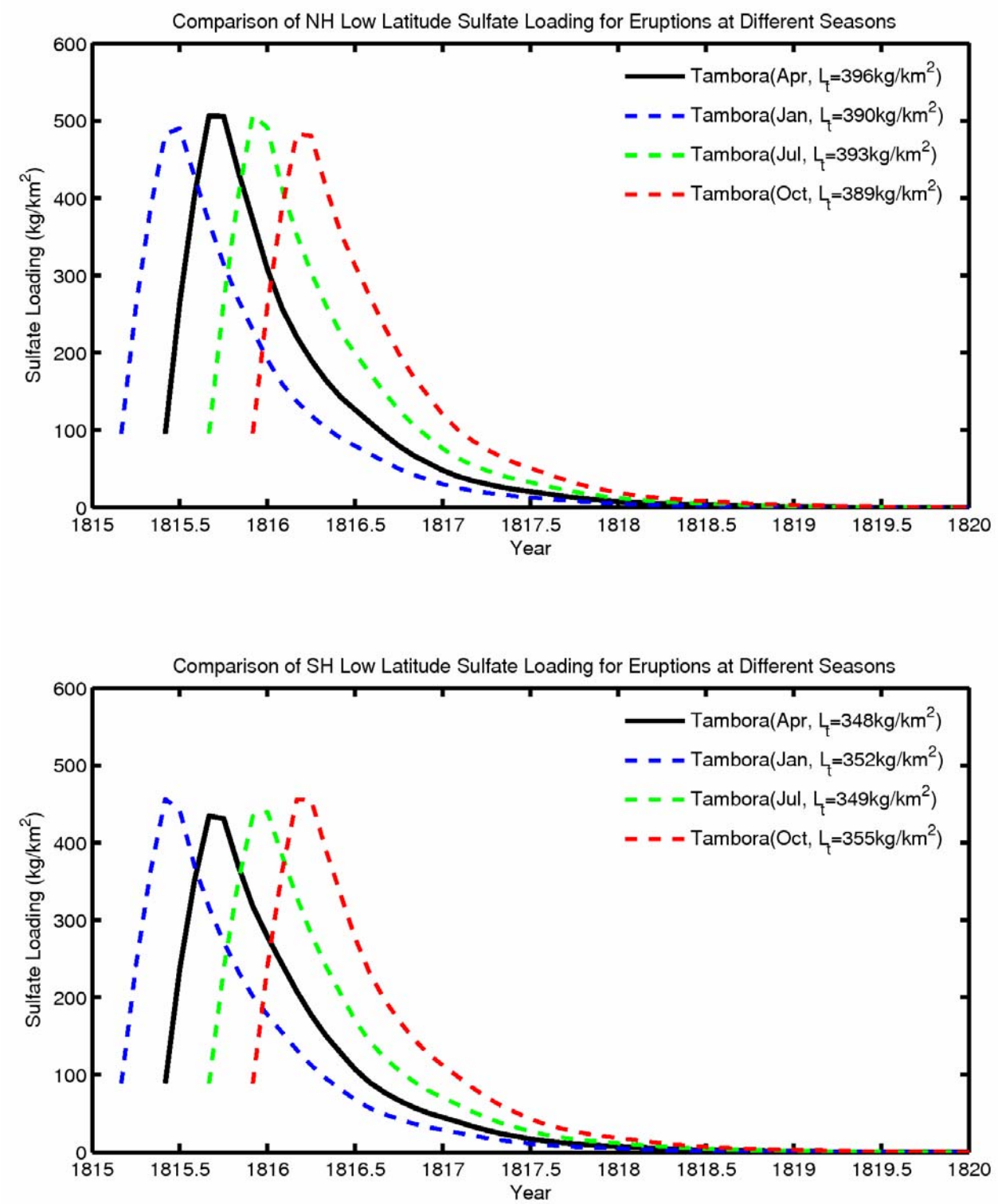

Figure 11. Low latitude sulfate loading for the Tambora eruption, assuming eruptions at different times of the year.